





# Valorization of *Passiflora ligularis* Shells for the Eco-Friendly Production of Zinc- and Copper-Oxide Nanoparticles

Daniela Camacho Valencia<sup>1</sup>; Ariadne Maria Tacusi Oblitas Taco<sup>2</sup>; Stamber Ramírez Revilla<sup>3</sup>;  
Gerson José Márquez<sup>4</sup>

<sup>1,2,3,4</sup>Universidad Tecnológica del Perú, Perú, [U19213681@utp.edu.pe](mailto:U19213681@utp.edu.pe), [sramirezr@utp.edu.pe](mailto:sramirezr@utp.edu.pe), [gmarquez@utp.edu.pe](mailto:gmarquez@utp.edu.pe)

<sup>1</sup>Universidad Nacional Agraria La Molina, Perú, [20240297@lamolina.edu.pe](mailto:20240297@lamolina.edu.pe)

**Abstract**– *Passiflora ligularis* (granadilla) is widely cultivated in tropical regions across the Americas. Its consumption generates waste, such as peels, that are typically discarded. In line with the principles of the circular economy, this study explores the green synthesis of metal oxide nanoparticles using granadilla shell extract, with potential applications in antimicrobial treatments and in the remediation of water contaminated with heavy metals or textile dyes. ZnO, CuO, and mixed Zn-Cu oxide nanoparticles were synthesized via an eco-friendly coprecipitation method, using the peel extract as a natural complexing and capping agent. The nanoparticles were characterized by electron diffraction, transmission electron microscopy, energy-dispersive X-ray spectroscopy, and infrared spectroscopy to determine their crystalline structure, morphology, size, aggregation state, and elemental composition. The nanoparticles obtained were ultra-small (3-5 nm), with low crystallinity. ZnO exhibited a hexagonal wurtzite structure, while CuO showed a monoclinic phase. The mixed Zn-Cu oxide displayed a Zn:Cu atomic ratio of approximately 1:3, corresponding to the formula  $\text{Zn}_{0.25}\text{Cu}_{0.75}\text{O}$ . The results suggest that granadilla shells are a viable green resource for synthesizing metal oxide nanoparticles with high specific surface areas, making them promising candidates for environmental and antimicrobial applications.

**Keywords**– granadilla, green synthesis, zinc oxide, copper oxide, nanoparticles.

## I. INTRODUCTION

Food systems generate substantial streams of inedible residues throughout the value chain. Global assessments reveal significant losses between harvest and retail, as well as considerable waste at both the retail and consumer levels. These findings have driven the development of circular strategies aimed at valorizing bio-residues into higher-value products, in alignment with SDG 12.3. In Peru, diagnostics have shown that materials with recovery potential constituted a large portion of the municipal solid waste stream in 2020. However, only about 1% of these materials were valorized, highlighting a critical implementation gap and underscoring the need for scalable upcycling pathways [1], [2]. At the same time, recent studies on food-waste biorefineries emphasize the importance of converting unavoidable by-products into functional materials that offer both environmental and economic benefits [3].

In this context, the *Passiflora* genus is economically and agronomically relevant in Latin America. The peel and seeds of *Passiflora ligularis* (granadilla) remain under-valorized

despite compositional profiles rich in phenolics and flavonoids with antioxidant capacity. Previous studies have reported the extraction of bioactive fractions from granadilla waste through sequential green extraction processes and have highlighted the antioxidant potential of *Passiflora* residues. These findings position granadilla peel as a promising renewable source of phytochemicals for the green synthesis of nanomaterials [4]–[9].

Green synthesis of nanomaterials replaces hazardous reagents with plant-based extracts that complex metal cations, steer nucleation, and cap the resulting nanoparticles. This approach enables a rapid and cost-effective production method aligned with the principles of frugal innovation. Several studies have demonstrated the feasibility and functional performance of *Passiflora* species in the green synthesis of metal-based nanoparticles [10]. For instance, copper nanoparticles with antimicrobial activity have been synthesized using *P. foetida* leaf extracts; copper oxide (CuO) nanoparticles with antioxidant properties and photocatalytic dye degradation capabilities have been produced using *P. edulis* extracts; and zinc oxide (ZnO) nanoparticles derived from *P. foetida* peels have shown effectiveness as catalysts for the removal of hazardous dyes [11]–[13]. Beyond feasibility, these works validate the role of phytochemicals as reducing and stabilizing agents.

Despite advances in the green synthesis of nanomaterials, studies specifically focused on zinc and copper oxide nanoparticles synthesized using *Passiflora ligularis* shell remain scarce. This contrasts with the broader body of research involving other *Passiflora* species or the synthesis of metallic and bimetallic nanoparticles. This gap is particularly noteworthy given that ZnO, CuO, and mixed Zn-Cu oxides exhibit complementary electronic properties and synergistic functionalities that are highly relevant for applications in catalysis, environmental remediation, and antimicrobial activity, areas where green synthesis offers added value, especially in resource-limited contexts [8], [9], [11]–[13].

Zinc oxide at the nanoscale is a semiconductor with a hexagonal wurtzite crystal structure and high physicochemical stability, attributes that account for its widespread use in chemical and gas sensors, biosensors, optoelectronic devices, and drug delivery systems [14]. Copper oxide, by contrast, crystallizes in the monoclinic tenorite structure. Functionally, CuO nanoparticles exhibit pronounced antimicrobial and

antifungal activity, primarily due to their ability to generate reactive oxygen species. Additionally, they are gaining attention as nanoagrochemicals (e.g., nanofertilizers and nanopesticides) and as nanopriming agents for seed enhancement and improved stress tolerance [15].

Recent studies indicate that combining ZnO and CuO in the form of nanocomposites or mixed oxides leads to synergistic effects, owing to favorable band alignment, enhanced charge separation and transfer, and greater structural stability. These features significantly improve their photocatalytic, antimicrobial, and sensing performance [16]. In this context, the synthesis of ZnO and CuO nanoparticles, as well as mixed Zn-Cu oxide nanoparticles, using granadilla shell extract is of particular interest. Furthermore, it is necessary to characterize the synthesized materials to evaluate their properties.

This study valorizes *Passiflora ligularis* shell through an eco-friendly coprecipitation method, in which the shell extract acts simultaneously as a complexing and capping agent to synthesize ZnO, CuO, and Zn-Cu mixed oxide nanoparticles. Structural, chemical, and morphological characterizations were carried out to assess the properties of the synthesized nanomaterials. The work presents a reproducible green synthesis protocol and underscores the potential of granadilla shells as a sustainable and value-added resource.

## II. METHODOLOGY

### A. Green Synthesis of Nanoparticles

ZnO, CuO, and Zn-Cu mixed oxide nanoparticles were synthesized via a green coprecipitation method using a hydroalcoholic extract derived from *Passiflora ligularis* shells as a reducing and capping agent. Fig. 1 summarizes the procedure followed for the synthesis of the nanoparticles. The first stage involves the selection, washing, drying, and grinding of the granadilla shells. After selecting the peels, the albedo was removed, and the shells were washed with distilled water. They were then air-dried for two days. Once dried, the shells were ground using a knife mill to obtain a fine and homogeneous powder.

To prepare the extract, 10 g of *Passiflora ligularis* shell powder was macerated in 100 mL of 90% ethanol. The mixture was first subjected to ultrasound-assisted extraction at 70 °C for 60 minutes. It was then filtered, concentrated by evaporation to a final volume of 50 mL, left to stand for 24 hours to allow decantation, and finally filtered again to obtain the working extract.

For each oxide, the corresponding nitrate precursor was used:  $\text{Zn}(\text{NO}_3)_2 \cdot 6\text{H}_2\text{O}$  for ZnO,  $\text{Cu}(\text{NO}_3)_2 \cdot 3\text{H}_2\text{O}$  for CuO, and a combination of both for the mixed oxide. These salts were dissolved in deionized water and stirred magnetically at 200 rpm while being heated to 80 °C for 25 minutes. In the case of the mixed oxide, the two metal salt solutions were first pre-homogenized at room temperature (200 rpm, 5 min), and then the combined solution was heated and stirred under the same conditions to promote ionic interaction.

The granadilla shell extract was added dropwise using a burette to the heated salt solution(s), followed by the addition of 2M sodium hydroxide (NaOH), which was initially added dropwise and subsequently added continuously. The reaction mixture was then left undisturbed for 1 hour. The final pH typically ranged between 10 and 11. The volumetric ratio of deionized water, hydroalcoholic extract, and NaOH was 1:1:1.

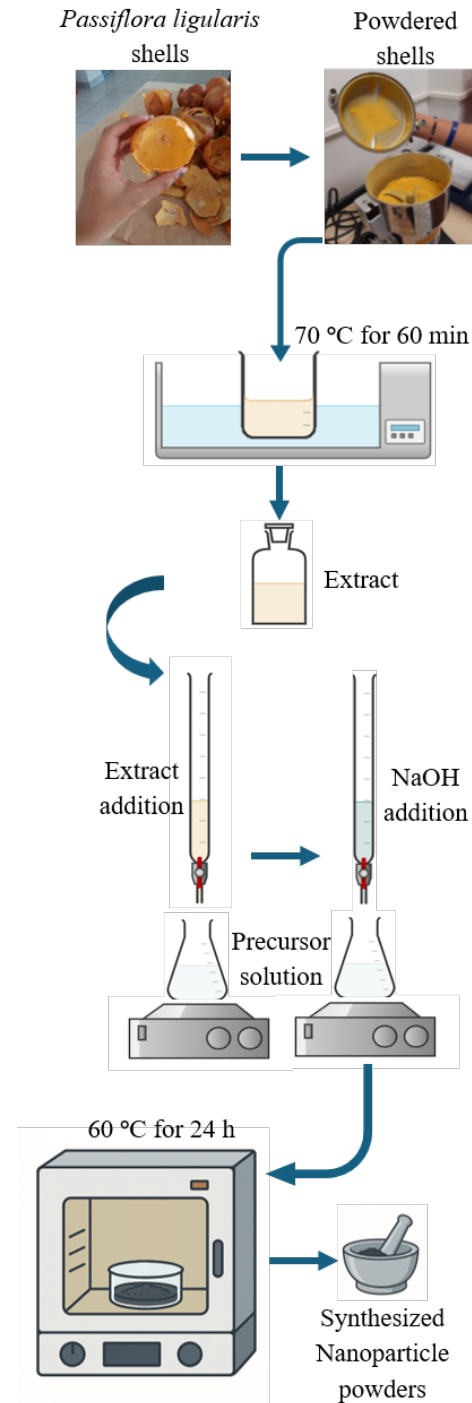


Fig. 1 Nanoparticle synthesis procedure using *P. ligularis* shell extract.

The resulting colloidal suspensions were allowed to cool, after which the supernatant was removed and the solid phase was collected by centrifugation at 4000 rpm for 10 minutes. The recovered solids were washed four times using 96% ethanol and deionized water, each time followed by vortexing and centrifugation at 4000 rpm for 5 minutes. Finally, the purified solids were resuspended in a small aliquot of ethanol, homogenized, and oven-dried at 60 °C for 24 hours to obtain the nanoparticle powders.

#### B. Characterization of Synthesized Nanoparticles

The crystal structure, morphology, size, and aggregation state of the nanoparticles were analyzed using a Thermo Scientific Talos F200i Transmission Electron Microscope (TEM), equipped with a field emission gun (FEG) and operated at an accelerating voltage of 200 kV. The samples were prepared using an alcohol-based solution to disperse the nanoparticles. Ultrasonic bath treatment was applied to achieve a uniform distribution. A microdroplet of the resulting dispersion was then deposited onto a copper grid for observation. Selected Area Electron Diffraction (SAED) was performed to identify the crystalline phases of the nanoparticles. Phase identification was carried out by comparing the ratios of the radii of the observed diffraction rings with the corresponding ratios of interplanar spacings ( $d_{hkl}$ ) obtained from crystallographic data in the Powder Diffraction File (PDF-2) database. The acquired micrographs were processed using DigitalMicrograph software, and more than 300 nanoparticles per sample were measured to evaluate the particle size distribution and determine the average particle size. The resulting size distributions were fitted to a log-normal function, and the mean particle size values were calculated and reported together with their corresponding standard deviations.

Elemental chemical analysis was carried out using Energy Dispersive Spectroscopy (EDS) on a Thermo Scientific Scios 2 DualBeam Scanning Electron Microscope (SEM). EDS measurements were performed on selected areas using the UltraDry detector.

The structural and chemical composition of the samples was analyzed by Fourier transform infrared spectroscopy (FTIR) using a Nicolet iN10 infrared microscope. Both reflection and ATR modes were employed, utilizing an MCT-B detector. The spectra were recorded in the range of 4000 to 600  $\text{cm}^{-1}$ .

### III. RESULTS AND DISCUSSIONS

#### A. Validation of the Green Synthesis and Yield

The validation of the synthesis process was based on reproducible macroscopic indicators, such as solution color changes upon basification and the formation of stable precipitates, as well as on the quantitative yields obtained under identical mixing, temperature, and pH conditions. Fig. 2 shows the reaction mixtures for the synthesis of the three metal oxides, both before and after the addition of the extract

and NaOH, where distinct color changes and precipitate formation can be observed. The final colors obtained are attributed to both the formation of nanoparticles and the presence of bioactive compounds from the phytochemical solution. For instance, in the case of zinc oxide, a precipitate was obtained which, after washing and drying, exhibited a light brown color, distinct from the typical white of pure ZnO [17], indicating that compounds from the *P. ligularis* shell extract remained associated with the nanoparticles, likely acting as an organic coating.

The yield from the initial syntheses, aimed at producing 200 mg of oxide, exceeded 72%. However, when scaling up the synthesis to produce 2 g of nanoparticles, yields greater than 90% were achieved. The observed losses are mainly attributed to material loss during washing and centrifugation cycles, and during nanoparticle recovery after drying. These losses are more pronounced when working with small quantities.

Furthermore, using the extract prepared from 10 g of *P. ligularis* shell powder, three separate syntheses yielding

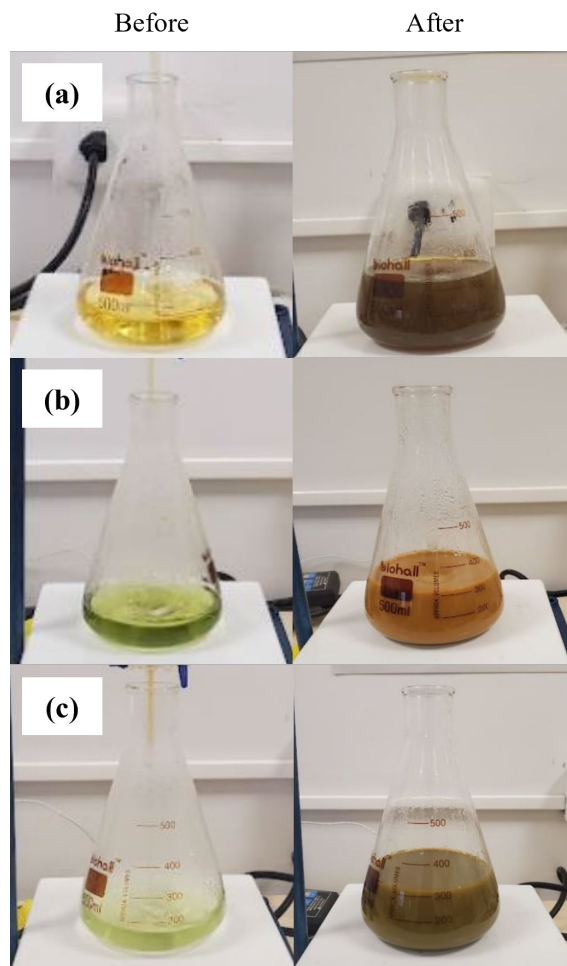


Fig. 2 Reaction mixture for the synthesis of (a) ZnO, (b) CuO, and (c) Zn-Cu mixed oxide nanoparticles, before and after adding the extract and NaOH.

approximately 2 g of nanoparticles each were successfully performed, demonstrating an extract productivity of ~6 g of nanoparticles per 10 g of shell powder, or equivalently, ~0.6 g of nanoparticles per gram of dry shell.

The Process Mass Intensity (PMI) was estimated to be approximately 30 g/g. The total mass considered in the PMI calculation included all reagents, solvents, and water used during the synthesis, but excluded the water employed exclusively for washing and cleaning operations. The resulting PMI value indicates a moderate level of material efficiency for the synthesis. Although this value is higher than those reported for optimized green processes (PMI < 10) [18], [19], it remains significantly lower than typical values observed in conventional nanoparticle synthesis routes [20]. Furthermore, the exclusive use of renewable biomass and benign solvents supports the classification of the process as a green synthesis pathway, with substantial potential for further optimization through solvent recovery and yield improvement.

Overall, these results confirm that the synthesis route illustrated in Fig. 1 is both reproducible and scalable, underscoring the value of *P. ligularis* shells as a recoverable biowaste suitable for the eco-friendly production of metal oxide nanoparticles.

#### B. Crystalline Structure of the Synthesized Nanoparticles

The electron diffraction patterns of the ZnO and CuO samples are shown in Fig. 3. The presence of poorly defined diffraction rings indicates low crystallinity, suggesting that both oxides may consist of very small nanoparticles. In such particles, structural disorder at the surface likely dominates over the order within the small crystalline domains. These results are consistent with previous studies reporting that nanoparticles synthesized at low temperatures are typically very small and either amorphous or poorly crystalline [21]. Thermal treatments at higher temperatures are often required to improve crystallinity, although this generally leads to an increase in particle size [22], [23].

The observed rings were indexed, as shown in Fig. 3, and were found to correspond to the main diffraction maxima of the hexagonal wurtzite structure (space group  $P6_3mc$ ) for ZnO and the monoclinic tenorite structure (space group  $C2/c$ ) for CuO, in agreement with the PDF-2 data sheets #36-1451 and #48-1548, respectively. Although phase confirmation was not performed using a more comprehensive crystallographic technique such as X-ray diffraction (XRD), the indexed SAED patterns closely matched the characteristic reflections of both ZnO and CuO phases, providing a reliable structural identification at the nanoscale. Future work will incorporate XRD measurements to more precisely assess the crystallinity and phase purity of the synthesized nanoparticles.

#### C. Morphology, Size, and Aggregation of the Synthesized Nanoparticles

Fig. 4 presents TEM micrographs of the three synthesized oxides. Two of the samples (ZnO and the Zn-Cu mixed oxide)

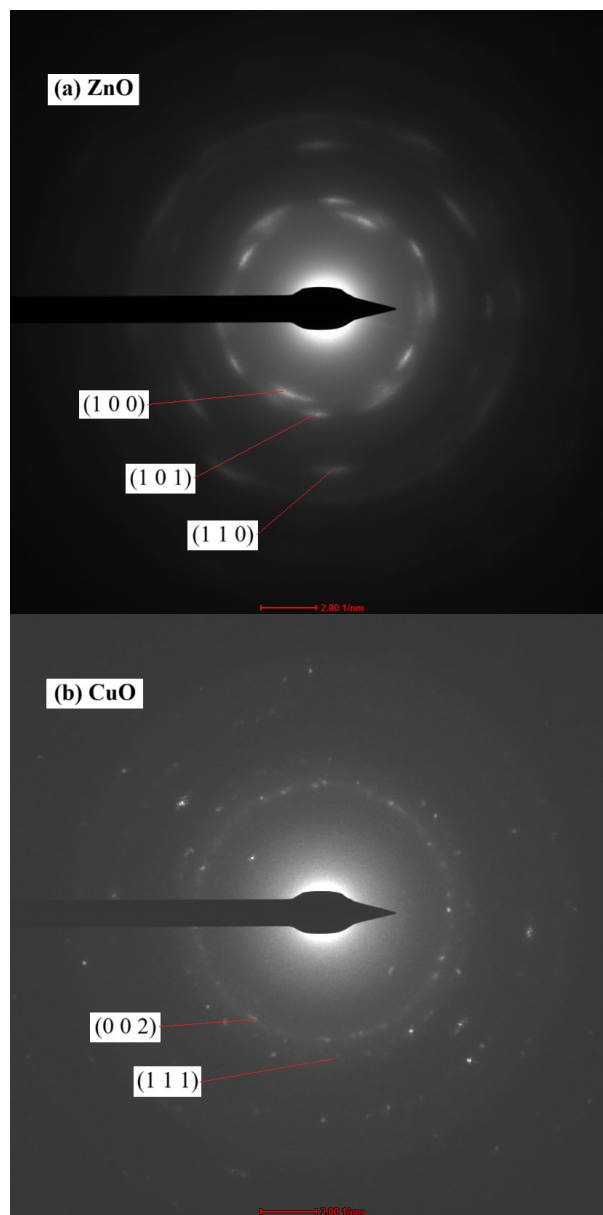


Fig. 3 Electron diffraction patterns of the synthesized nanoparticles of (a) ZnO and (b) CuO.

exhibit predominantly irregularly shaped nanoparticles, whereas the CuO nanoparticles display an approximately spherical morphology. In all three nanomaterials, the particles appear densely packed, with a particularly high degree of aggregation observed in ZnO and the Zn-Cu mixed oxide. This pronounced aggregation is likely driven by van der Waals interactions [24]. As reported in the literature, nanoscale particles inherently exhibit a strong tendency to aggregate, a phenomenon further promoted during the drying step required to obtain the nanoparticle powders [25]. To mitigate nanoparticle agglomeration, future optimization of the synthesis could focus on pH control and improving colloidal stability.



The micrographs also suggest that these aggregates are embedded within or coated by an additional layer, similar to the nanoaggregates reported in previous studies [26]; this coating likely corresponds to an organic matrix derived from the *P. ligularis* shell extract. The presence of this organic layer is expected to enhance the stability of the nanoparticles when dispersed as a colloidal suspension by introducing steric and electrostatic repulsion forces [27], [28]. Moreover, its surface functional groups could further improve the adsorption capacity and catalytic performance of the nanomaterials in environmental remediation or antimicrobial applications.

Particle size distributions for the three oxide samples are shown in Fig. 5. The results indicate that the nanocomposites consist of particles ranging from 1 to 11 nm in diameter, following log-normal distributions, with mean sizes of approximately 5 nm for ZnO and around 3 nm for both CuO and the Zn-Cu mixed oxide. These findings confirm the formation of ultrasmall nanoparticles, consistent with the low crystallinity inferred from the SAED analysis, and are in good agreement with previous reports of similarly sized particles produced via green synthesis routes [29], [30].

The particle size distributions exhibited low standard deviations ( $\sigma = 0.28, 0.34$ , and  $0.22$ ), indicating narrow size distributions and effective control over nucleation and growth during the green synthesis process. Such low dispersion values demonstrate a high degree of size uniformity among the nanoparticles. Moreover, since all  $\sigma$  values are below 0.4, the samples can be classified as quasi-monodisperse, a characteristic that is desirable for applications in which size-dependent properties are critical.

The ultrasmall dimensions of the nanoparticles suggest a high specific surface area, potentially exceeding  $80 \text{ m}^2/\text{g}$ , as reported for ultrasmall ZnO nanoparticles [31]. However, the pronounced aggregation observed may reduce the accessible surface area, with reported values in similar systems falling below  $50 \text{ m}^2/\text{g}$  due to agglomeration effects [32]. Future work will include Brunauer–Emmett–Teller (BET) surface area measurements to quantitatively evaluate this parameter and establish its relationship with nanoparticle aggregation.

#### D. Elemental and Functional Group Composition of the Synthesized Nanoparticles

SEM images of the three synthesized oxides are shown in Fig. 6, with the regions selected for elemental analysis indicated. In all three samples, area #1 corresponds to large aggregates of nanocomposite particles, area #2 to smaller aggregates, and area #3 (darker regions) to the material coating the nanoparticles.

The results of the EDS analysis for these three regions in each sample are presented in Table I. In addition to the expected elements (oxygen, zinc, and copper) other elements such as carbon (C), magnesium (Mg), phosphorus (P), potassium (K), and calcium (Ca) were also detected. These elements originate from the chemical composition of the *Passiflora ligularis* shell extract, which forms the organic material coating the nanoparticles. After oxygen, carbon was

the most abundant element, indicating a significant presence of organic matter in the nanocomposites.

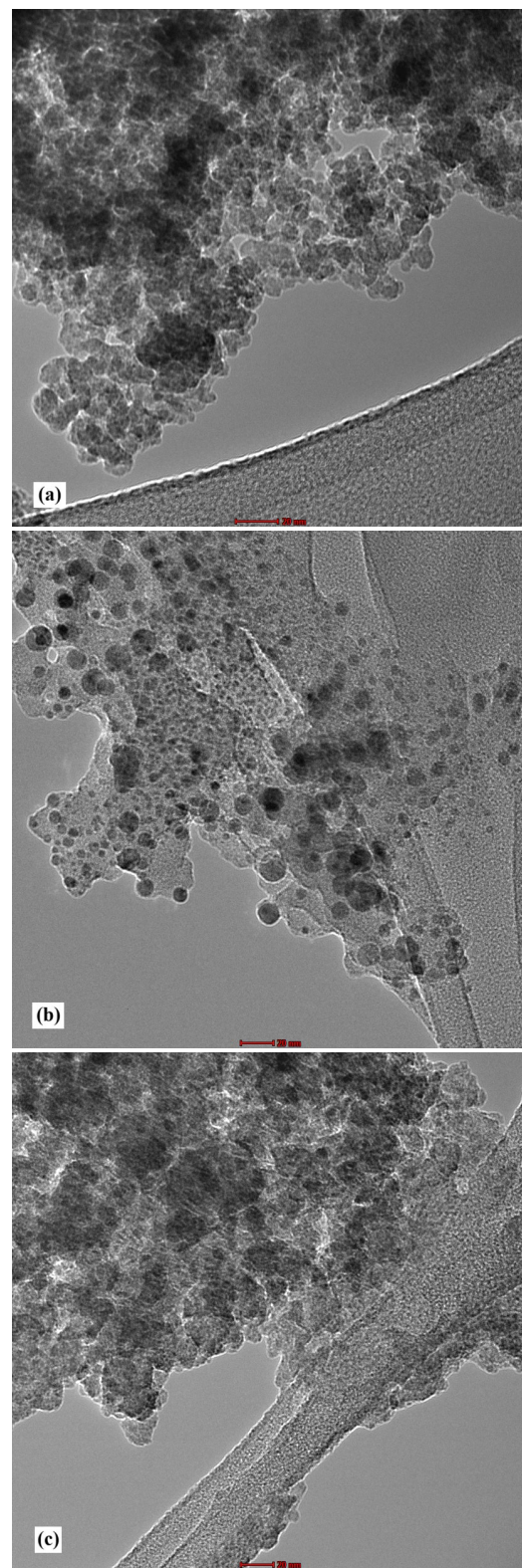


Fig. 4 TEM images of the synthesized nanoparticles: (a) ZnO, (b) CuO, (c) Zn-Cu mixed oxide. All scale bars correspond to 20 nm.

The analysis of area #3 confirms that the coating material is indeed an organic compound derived from the *P. ligularis* shell extract, consistent with the findings from the TEM analysis. In the case of the mixed Zn-Cu oxide, the ratio of the atomic percentages of Cu to Zn is approximately 3:1, suggesting a stoichiometry that can be represented by the formula  $\text{Zn}_{0.25}\text{Cu}_{0.75}\text{O}$ .

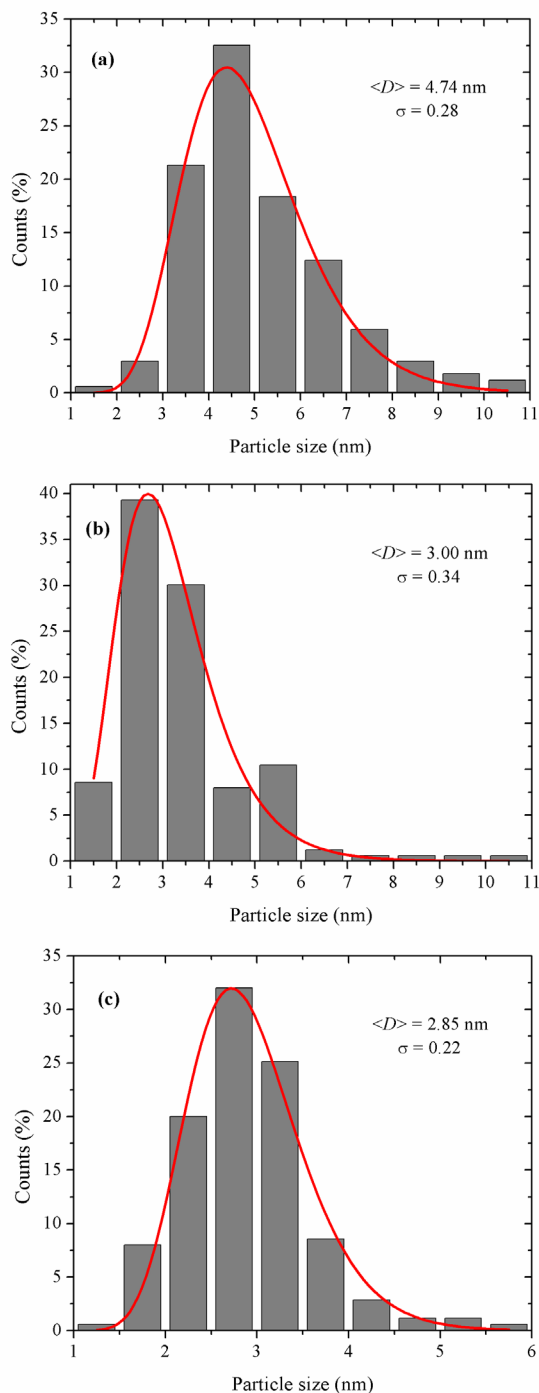


Fig. 5 Particle size distributions of the synthesized nanoparticles: (a) ZnO, (b) CuO, and (c) Zn-Cu mixed oxide.

The FTIR spectra of ZnO, CuO, and Zn-Cu mixed oxide nanoparticles synthesized using *Passiflora ligularis* shell extract are shown in Fig. 7. These spectra exhibit similar profiles in the high- and mid-wavenumber regions, reflecting the presence of phytochemicals from the extract that act as both reducing and stabilizing agents.

The positions of the absorption bands observed in the spectra are listed in Table II, along with their corresponding vibrational assignments. A broad absorption band at approximately  $3380\text{--}3430\text{ cm}^{-1}$  is attributed to O–H stretching vibrations of alcohols, phenols, and adsorbed water molecules, features commonly associated with surface stabilization in biogenic metal oxides [12], [13]. Peaks near  $2920$  and  $2850\text{ cm}^{-1}$  correspond to asymmetric and symmetric stretching vibrations of aliphatic C–H bonds, indicating the presence of organic residues from the extract.

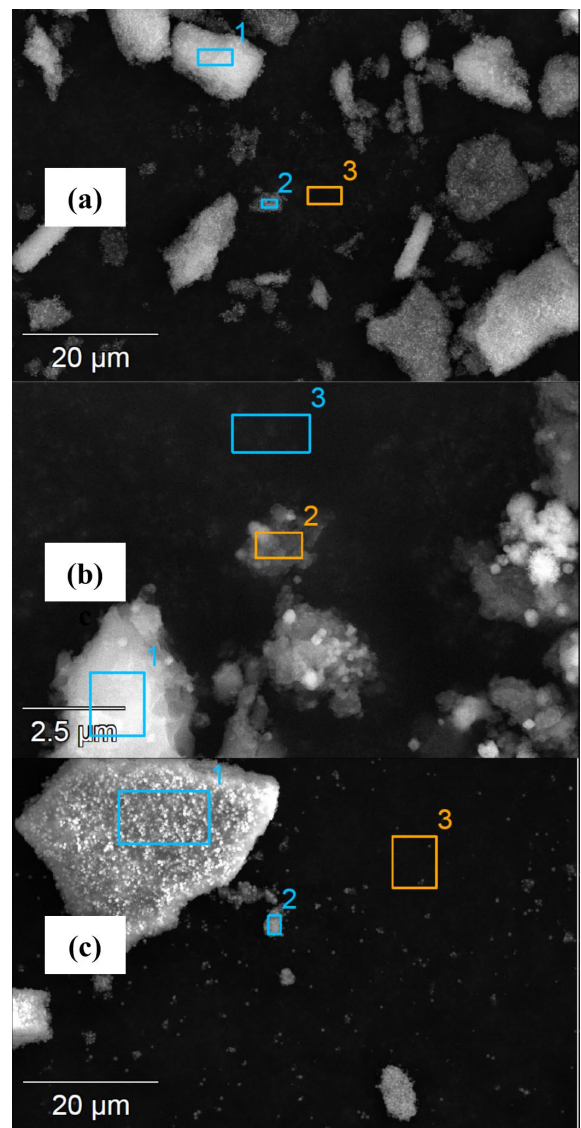


Fig. 6 SEM micrographs showing the areas selected for EDS analysis of the synthesized nanoparticles: (a) ZnO, (b) CuO, and (c) Zn-Cu mixed oxide.

TABLE I  
ATOMIC PERCENTAGES OBTAINED BY EDS ANALYSIS OF THE  
SYNTHESIZED NANOPARTICLES IN THE AREAS (A) MARKED IN FIG. 6

Sample	A	Atomic percentage (%)							
		C	O	Mg	P	K	Ca	Zn	Cu
ZnO	1	26.48	63.96	0.25	0.99	0.07	0.25	7.99	-
	2	31.76	66.03	0.06	0.20	-	0.05	1.92	-
	3	33.33	66.67	-	-	-	-	-	-
CuO	1	31.55	66.40	0.08	0.36	-	0.10	-	1.51
	2	32.53	66.04	-	0.13	-	-	-	1.30
	3	33.33	66.67	-	-	-	-	-	-
Zn-Cu oxide	1	14.51	53.40	0.63	1.69	0.16	0.56	8.71	20.33
	2	29.55	63.90	0.11	0.27	0.11	0.09	1.41	4.56
	3	33.30	66.63	-	-	-	-	-	0.07

The absorption band at  $\sim 1620\text{--}1650\text{ cm}^{-1}$  can be attributed to overlapping aromatic C=C stretching and C=O stretching from amide groups, suggesting the presence of both phenolic compounds and proteinaceous residues functioning as capping agents. The band at  $\sim 1480\text{ cm}^{-1}$  corresponds to aliphatic C-H bending, while the signal near  $1400\text{ cm}^{-1}$  is associated with symmetric and asymmetric stretching of carboxylate groups ( $\text{COO}^-$ ), likely originating from polyphenolic acids. The absorption band observed around  $1280\text{ cm}^{-1}$  corresponds to C-O stretching vibrations in carboxylic acids, phenols, or esters present in the *Passiflora ligularis* shell extract. Bands observed in the  $1000\text{--}1100\text{ cm}^{-1}$  region are assigned to O-H bending vibrations, related to molecular water or surface hydroxyl groups.

TABLE II  
FTIR BAND POSITIONS AND VIBRATIONAL ASSIGNMENTS FOR THE  
SYNTHESIZED NANOPARTICLES

Band position ( $\text{cm}^{-1}$ )	Vibrational assignment
3380 - 3430	O-H stretching
$\sim 2920$	C-H asymmetric stretching
$\sim 2850$	C-H symmetric stretching
1620 - 1650	C=C / C=O stretching
$\sim 1480$	C-H bending
$\sim 1400$	$\text{COO}^-$ symmetric stretching
$\sim 1280$	C-O stretching
1000 - 1100	O-H bending
800 - 850	Zn-O / Cu-O stretching
$\sim 760$	Cu-O stretching

In the low-wavenumber region, distinct metal-oxygen vibrations were observed for each oxide. For CuO, a band at approximately  $760\text{ cm}^{-1}$  is attributed to Cu-O stretching vibrations, consistent with the findings of Yasin et al. [13]. For ZnO, although Khan et al. [12] reported a Zn-O stretching band below  $500\text{ cm}^{-1}$ , a weak feature near  $600\text{ cm}^{-1}$  in the present spectrum can also be attributed to Zn-O vibrations, which has been documented in other green-synthesized ZnO nanoparticles [33]. In the Zn-Cu mixed oxide, a broad band spanning approximately  $800\text{--}850\text{ cm}^{-1}$  was observed, indicating the presence of both Zn-O and Cu-O stretching modes. This broadening may suggest lattice integration of  $\text{Zn}^{2+}$  and  $\text{Cu}^{2+}$  ions, supporting the formation of a mixed oxide phase rather than a simple physical mixture.

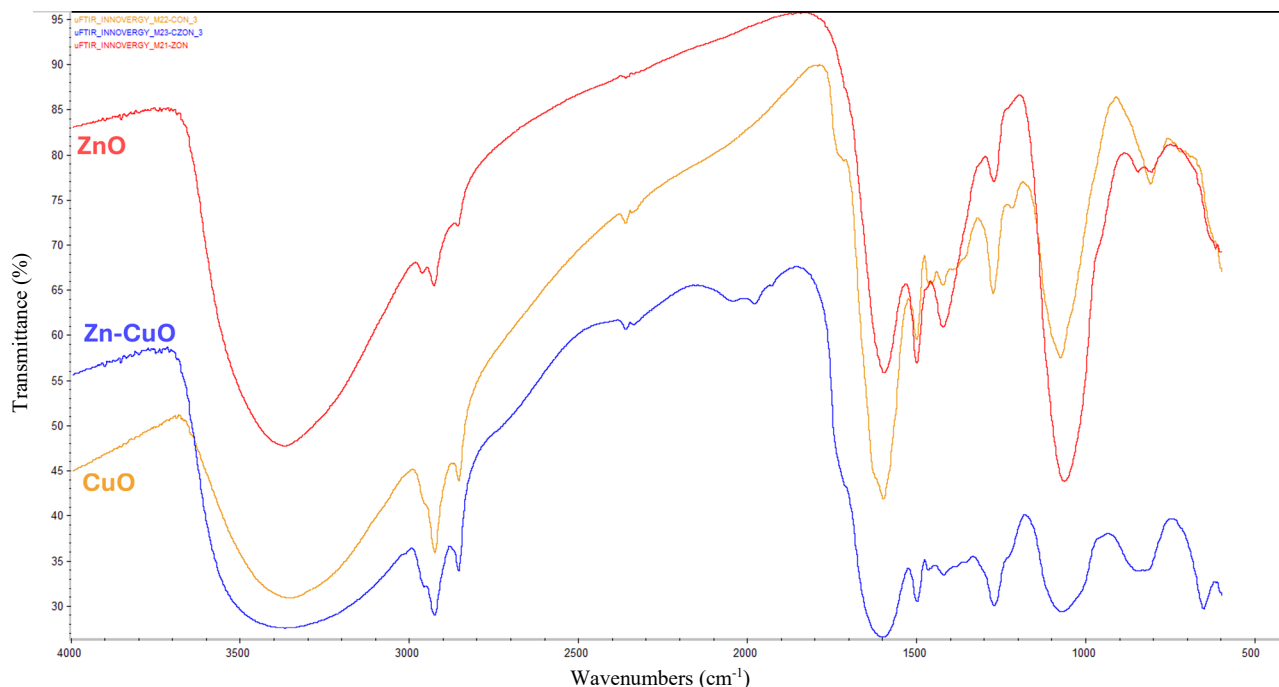


Fig. 7 FTIR spectra of the synthesized ZnO, CuO, and Zn-Cu mixed oxide (Zn-CuO) nanoparticles.



Although functional validation through photocatalytic assays was beyond the scope of this study, the ultrasmall particle size and chemical composition of the synthesized nanocomposites suggest a high catalytic potential for the removal of aqueous contaminants. Future work will involve conducting comparative experiments to rigorously evaluate their catalytic efficiency in degrading textile dyes from wastewater.

#### IV. CONCLUSIONS

A low-temperature green synthesis route using *Passiflora ligularis* shell extract enabled the reliable production of ZnO, CuO, and Zn-Cu mixed oxide nanoparticles with high yields (>90% at gram scale) and an extract productivity of approximately 0.6 g of nanoparticles per gram of powdered shell, supporting both the scalability and circular valorization of this biowaste. Ultra-small nanoparticles were obtained, with average sizes of ~5 nm for ZnO and ~3 nm for both CuO and the Zn-Cu mixed oxide, consistent with the low crystallinity observed in the nanomaterials. Despite this, the expected crystal structures (hexagonal wurtzite for ZnO and monoclinic tenorite for CuO) were confirmed. The nanoparticles exhibited pronounced aggregation and were coated with an organic layer derived from the *P. ligularis* shell extract. For the mixed oxide, elemental analysis revealed a Cu:Zn atomic ratio of approximately 3:1 in representative regions, suggesting an overall composition close to  $\text{Zn}_{0.25}\text{Cu}_{0.75}\text{O}$ . FTIR spectra of all powders showed characteristic phytochemical bands, while the low-wavenumber region revealed metal-oxygen vibrations, confirming both the presence of an organic coating and the successful formation of metal oxides.

#### ACKNOWLEDGMENT

The authors would like to thank the Universidad Tecnológica del Perú for financial support through project P-2023-SUR-01. They also extend their gratitude to Dr. Hugo Guillermo Jiménez Pacheco from the INNOVERGY Institute at the Universidad Católica de Santa María, Arequipa, Peru, for his assistance with the infrared spectroscopy measurements.

#### REFERENCES

- [1] Food and Agriculture Organization of the United Nations, "The State of Food and Agriculture 2019. Moving forward on food loss and waste reduction," 2019, *FAO Rome, Rome*. [Online]. Available: [www.fao.org/publications](http://www.fao.org/publications)
- [2] ComexPerú - Sociedad de Comercio Exterior del Perú, "Solo aprovechamos el 1% de residuos orgánicos e inorgánicos que generamos," 2022. [Online]. Available: <https://www.comexperu.org.pe/articulo/solo-aprovechamos-el-1-de-residuos-organicos-e-inorganicos-que-generamos>
- [3] D. A. Teigiserova, L. Hamelin, and M. Thomsen, "Review of high-value food waste and food residues biorefineries with focus on unavoidable wastes from processing," *Resour. Conserv. Recycl.*, vol. 149, pp. 413–426, Oct. 2019, doi: 10.1016/j.resconrec.2019.05.003.
- [4] R. Vardanega, F. S. Fuentes, J. Palma, W. Bugueño-Muñoz, P. Cerezal-Mezquita, and M. C. Ruiz-Domínguez, "Valorization of granadilla waste (*Passiflora ligularis*, Juss.) by sequential green extraction processes based on pressurized fluids to obtain bioactive compounds," *J. Supercrit. Fluids*, vol. 194, p. 105833, Mar. 2023, doi: 10.1016/j.supflu.2022.105833.
- [5] M. M. Bonilla Morales, A. C. Aguirre Morales, and O. M. Agudelo Varela, "Passiflora morphology: a guide for the description of species," *Rev. Investig. Agrar. y Ambient.*, vol. 6, no. 1, pp. 91–110, 2015.
- [6] N. Linares-Devia, J. Arrieta-Escobar, Y. Baena, A. Orjuela, and C. Osorio, "Development and Characterization of Emulsions Containing Ground Seeds of Passiflora Species as Biobased Exfoliating Agents," *Cosmetics*, vol. 9, no. 1, p. 15, Jan. 2022, doi: 10.3390/cosmetics9010015.
- [7] S. Wiliantari, R. Iswandana, and B. Elya, "Total Polyphenols, Total Flavonoids, Antioxidant Activity and Inhibition of Tyrosinase Enzymes from Extract and Fraction of Passiflora ligularis Juss.," *Pharmacogn. J.*, vol. 14, no. 3, pp. 672–680, Jun. 2022, doi: 10.5530/pj.2022.14.86.
- [8] G. Domínguez-Rodríguez, M. C. García, M. Plaza, and M. L. Marina, "Revalorization of Passiflora species peels as a sustainable source of antioxidant phenolic compounds," *Sci. Total Environ.*, vol. 696, p. 134030, Dec. 2019, doi: 10.1016/j.scitotenv.2019.134030.
- [9] M. N. Marroquin, S. M. Cruz, and A. Cáceres, "Antioxidant activity and phenolic compounds in three species of Passifloraceae (*Passiflora edulis*, *P. incarnata*, *P. ligularis*) from Guatemala," *Acta Hort.*, no. 964, pp. 93–98, Oct. 2012, doi: 10.17660/ActaHortic.2012.964.11.
- [10] T. My-Thao Nguyen *et al.*, "Biosynthesis of metallic nanoparticles from waste Passiflora edulis peels for their antibacterial effect and catalytic activity," *Arab. J. Chem.*, vol. 14, no. 4, p. 103096, Apr. 2021, doi: 10.1016/j.arabjc.2021.103096.
- [11] S. Renganathan, S. Fatma, and K. P., "Green synthesis of copper nanoparticle from Passiflora foetida leaf extract and its antibacterial activity," *Asian J. Pharm. Clin. Res.*, vol. 10, no. 4, p. 79, Apr. 2017, doi: 10.22159/ajpcr.2017.v10i4.15744.
- [12] M. Khan, P. Ware, and N. Shimpi, "Synthesis of ZnO nanoparticles using peels of Passiflora foetida and study of its activity as an efficient catalyst for the degradation of hazardous organic dye," *SN Appl. Sci.*, vol. 3, no. 5, p. 528, May 2021, doi: 10.1007/s42452-021-04436-4.
- [13] A. Yasin *et al.*, "Fabrication of Copper Oxide Nanoparticles Using Passiflora edulis Extract for the Estimation of Antioxidant Potential and Photocatalytic Methylene Blue Dye Degradation," *Agronomy*, vol. 12, no. 10, p. 2315, Sep. 2022, doi: 10.3390/agronomy12102315.
- [14] B. Cheviri, A. Vijayan, M. Radhakrishnan, A. Unnikrishnan, M. J. Prambath, and S. S. Nair, "Harnessing the multifunctional properties of ZnO nanoparticles for High-Performance optical and Paper-printed colorimetric detection of silver ions," *Mater. Sci. Eng. B*, vol. 322, p. 118618, Dec. 2025, doi: 10.1016/j.mseb.2025.118618.
- [15] N. Amin and K. Aziz, "Copper oxide-based nanoparticles in agrotechnology: advances and applications for sustainable farming," *Agric. Food Secur.*, vol. 14, no. 1, p. 7, May 2025, doi: 10.1186/s40066-025-00530-7.
- [16] S. Ngwenya *et al.*, "Eco-friendly synthesis of ZnO, CuO, and ZnO/CuO nanoparticles using extract of spent Pleurotus ostreatus substrate, and their antioxidant and anticancer activities," *Discov. Nano*, vol. 20, no. 1, p. 35, Feb. 2025, doi: 10.1186/s11671-025-04199-6.
- [17] X. Xiao, G. Hu, Y. Liang, P. Yan, and A. Jiang, "A Review on the Properties of Zinc Oxide Nanoparticles in Various Industries and Biomedical Fields: Enhancing Chemical and Physical Characteristics," *Iran. J. Chem. Chem. Eng.*, vol. 43, no. 1, pp. 46–65, 2024, doi: 10.30492/ijcce.2023.1990407.5889.
- [18] A. U. Pandya, M. P. Chaudhari, V. S. Sharma, A. George, G. N. Shiyal, and P. S. Shrivastav, "Application of Fe<sub>3</sub>O<sub>4</sub>@MCC Nanoparticles as a Heterogeneous Catalyst for Sustainable Multicomponent Synthesis of 2,3'-Biindoles," *ChemCatChem*, vol. 17, no. 1, Jan. 2025, doi: 10.1002/cctc.202401308.
- [19] S. Kohli, G. Rathee, S. Hooda, and R. Chandra, "An efficient approach for the green synthesis of biologically active 2,3-dihydroquinazolin-4(1H)-ones using a magnetic EDTA coated copper based nanocomposite," *RSC Adv.*, vol. 13, no. 3, pp. 1923–1932, 2023, doi: 10.1039/D2RA07496F.
- [20] A. García-Quintero and M. Palencia, "A critical analysis of environmental sustainability metrics applied to green synthesis of



- nanomaterials and the assessment of environmental risks associated with the nanotechnology,” *Sci. Total Environ.*, vol. 793, p. 148524, Nov. 2021, doi: 10.1016/j.scitotenv.2021.148524.
- [21] S. Mishra, B. K. Pandey, S. Dwivedi, M. Jaiswal, and R. Dhar, “Green synthesis of amorphous and crystalline copper oxide nanoparticles and their photocatalytic and antioxidant activities,” *J. Alloys Compd.*, vol. 1033, p. 181210, Jun. 2025, doi: 10.1016/j.jallcom.2025.181210.
- [22] E. Pérez, G. Marquez, and V. Sagredo, “Effect of Calcination on Characteristics of Nickel Ferrite Nanoparticles Synthesized by Sol-Gel Method,” *Iraqi J. Appl. Phys.*, vol. 15, no. 1, pp. 13–17, 2019.
- [23] G. Márquez, V. Sagredo, R. Guillén-Guillén, G. Attolini, and F. Bolzoni, “Calcination effects on the crystal structure and magnetic properties of CoFe<sub>2</sub>O<sub>4</sub> nanopowders synthesized by the coprecipitation method,” *Rev. Mex. Fis.*, vol. 66, no. 3, pp. 251–257, 2020, doi: 10.31349/REVMEXFIS.66.251.
- [24] M. Manimaran, M. N. Norizan, M. H. M. Kassim, M. R. Adam, N. Abdullah, and M. N. F. Norrahim, “Critical review on the stability and thermal conductivity of water-based hybrid nanofluids for heat transfer applications,” *RSC Adv.*, vol. 15, no. 18, pp. 14088–14125, 2025, doi: 10.1039/D5RA00844A.
- [25] E. Santiago, G. Marquez, R. Guillen-Guillen, C. Jaimes, V. Sagredo, and G. E. Delgado, “Characterization of hematite and Ni-Zn mixed ferrites nanocomposites synthesized by the coprecipitation method,” *Rev. Latinoam. Metal. y Mater.*, vol. 40, no. 1, pp. 49–58, 2020, [Online]. Available: <http://www.rlmm.org/ojs/index.php/rlmm/article/view/984>
- [26] F. Morales, G. Márquez, V. Sagredo, T. E. Torres, and J. C. Denardin, “Structural and magnetic properties of silica-coated magnetite nanoaggregates,” *Phys. B Condens. Matter*, vol. 572, pp. 214–219, 2019, doi: 10.1016/j.physb.2019.08.007.
- [27] J. Lee *et al.*, “Delineating the role of surface grafting density of organic coatings on the colloidal stability, transport, and sorbent behavior of engineered nanoparticles,” *Environ. Sci. Nano*, vol. 11, no. 2, pp. 578–587, 2024, doi: 10.1039/D3EN00358B.
- [28] J. Liu *et al.*, “Comparative study on effects of pH, electrolytes, and humic acid on the stability of acetic and polyacrylic acid coated magnetite nanoparticles,” *Chemosphere*, vol. 319, p. 137992, Apr. 2023, doi: 10.1016/j.chemosphere.2023.137992.
- [29] M. A. Dheyab *et al.*, “Turning food waste-derived ultrasmall gold nanoparticles as a photothermal agent for breast cancer cell eradication,” *Inorg. Chem. Commun.*, vol. 169, p. 113030, Nov. 2024, doi: 10.1016/j.inoche.2024.113030.
- [30] B. Yang, F. Qi, J. Tan, T. Yu, and C. Qu, “Study of Green Synthesis of Ultrasmall Gold Nanoparticles Using Citrus Sinensis Peel,” *Appl. Sci.*, vol. 9, no. 12, p. 2423, Jun. 2019, doi: 10.3390/app9122423.
- [31] R. Chen, J. Wang, and L. Xiang, “Facile synthesis of mesoporous ZnO sheets assembled by small nanoparticles for enhanced NO<sub>2</sub> sensing performance at room temperature,” *Sensors Actuators B Chem.*, vol. 270, pp. 207–215, Oct. 2018, doi: 10.1016/j.snb.2018.05.005.
- [32] J. Guo, H. Yu, D. Wang, G. Chen, and L. Fan, “Experimental study, mechanism, and process optimization of hydrodynamic cavitation-enhanced green synthesis of nano ZnO using Eupatorium Adenophorum,” *Chem. Eng. Process. - Process Intensif.*, vol. 214, p. 110330, Aug. 2025, doi: 10.1016/j.cep.2025.110330.
- [33] A. Jayachandran, A. T.R., and A. S. Nair, “Green synthesis and characterization of zinc oxide nanoparticles using Cayratia pedata leaf extract,” *Biochem. Biophys. Reports*, vol. 26, p. 100995, Jul. 2021, doi: 10.1016/j.bbrep.2021.100995.